This paper describes objective technical results and analysis. Any subjective views or opinions that might be expressed in the paper do not necessarily represent the views of the U.S. Department of Energy or the United States Government.

SAND2021-1903J

The Inductively Driven Transmission Line: A passively coupled device for diagnostic applications on the Z Pulsed Power Facility

Clayton E. Myers,[1, a)] Derek C. Lamppa,[1] Christopher A. Jennings,[1] Matthew R. Gomez,[1] Patrick F. Knapp,[1] Michael Kossow,[1] Larry M. Lucero,[1] James K. Moore,[1] and David A. Yager-Elorriaga[1]
[1] *Sandia National Laboratories, Albuquerque, NM 87185 USA*

(Dated: 3 February 2021)

The inductively driven transmission line (IDTL) is a miniature current-carrying device that passively couples to fringe magnetic fields in the final power feed on the Z Pulsed Power Facility. The IDTL redirects a small amount of Z's magnetic energy along a secondary path to ground, thereby enabling pulsed power diagnostics to be driven in parallel with the primary load for the first time. IDTL experiments and modeling presented here indicate that IDTLs operate non-perturbatively on Z and that they can draw in excess of 150 kA of secondary current, which is enough to drive an X-pinch backlighter. Additional experiments show that IDTLs are also capable of making cleaner, higher-fidelity measurements of the current flowing in the final feed.

I. INTRODUCTION

The Z Pulsed Power Facility routinely delivers a >20 MA, 100 ns pulse of electrical current to centimeter-scale imploding loads.[1] This current pulse fills the final 5 cm of the power feed with ∼3 MJ of magnetic energy. If even a small amount of this magnetic energy can be non-perturbatively redirected along a secondary path to ground, valuable pulsed-power-driven diagnostics could be fielded in parallel with the primary load. One such diagnostic is the X-pinch backlighter,[2,3] which can be used for both penetrating radiography[4–7] and X-ray diffraction.[8] While X-pinches are routinely used as diagnostic tools on smaller pulsed power facilities,[6,9–12] they have never been fielded on Z due to the inductive and geometric constraints associated with delivering >20 MA of current to the primary load. In this paper, we introduce a new device—the inductively driven transmission line (IDTL)—that is capable of redirecting >150 kA of current along a secondary path to ground without perturbing the primary load. The experimental results presented here demonstrate that IDTLs enable two groundbreaking diagnostic applications on Z: (1) high-current IDTLs can draw enough current to drive diagnostic X-pinches in parallel with the primary load; and (2) low-current IDTLs can generate cleaner, higher-fidelity measurements of the current flowing in the final feed.

The IDTL is a single-turn transformer that is coupled to fringe magnetic fields that are present in the final power feed on Z. As shown in Fig. 1a, these fringe fields are found in centimeter-scale holes that are routinely cut in the top anode to provide access for B-dot sensors to measure the magnetic field and therefore the current in the final feed.[13] The standard Z B-dot sensor shown in Fig. 1a is comprised of a passive B-dot loop housed in a flux-reducing copper cavity that limits the voltage induced on the sensor. IDTLs, on the other hand, contain a single-turn copper drive loop that protrudes downward into the anode hole and robustly couples to the available fringe magnetic fields (see Figs. 1b and 1c). The resulting induced voltage drives tens or hundreds of kiloamperes of secondary current into a short coaxial transmission line that is embedded in the copper body of the IDTL.

II. IDTL DESIGN AND MODELING

The two key factors that determine how much of Z's magnetic flux can be coupled to an IDTL are (1) the size of the anode hole to which the IDTL is mounted; and (2) the geometry of the IDTL drive loop within that anode hole. A larger hole increases the strength of the available fringe fields and accommodates a larger drive loop, but it also increases the risk of perturbing the primary power flow in the final feed. To explore these trade-offs, we designed and tested two types of IDTLs: The first is the compact IDTL shown in Fig. 1b. This low-flux, low-current design mounts to a circular hole in the anode that is not much larger than the standard B-dot hole shown in Fig. 1a (12.7 mm versus 9.1 mm diameter). The drive loop is constructed from 1.5 mm-diameter copper wire and drops to within 2 mm of the anode power flow surface. Two B-dot loops (only one of which is shown) measure the magnetic field generated by the induced IDTL current. The second IDTL tested here, which is shown in Fig. 1c, is a high-flux, high-current design. This larger IDTL mounts to a 30 mm-long anode slot whose out-of-plane width varies from 10–15 mm. The slot enables a ∼23 mm segment of the drive loop, which is constructed from 2.9 mm-diameter copper wire, to run within 2 mm of the anode power flow surface and couple substantially more magnetic flux to the IDTL. Two stacked B-dot loops measure the induced current, which is expected to exceed 150 kA in this high-current IDTL design.

To quantify how much current I and voltage V are expected to be generated by each IDTL, we examine the standard L-R circuit equation:

$$V = -\frac{d\Phi_Z}{dt} = -M_Z\frac{dI_Z}{dt} = RI + L\frac{dI}{dt}, \qquad (1)$$

[a)] Electronic mail: cemyers@sandia.gov

Sandia National Laboratories is a multimission laboratory managed and operated by National Technology & Engineering Solutions of Sandia, LLC, a wholly owned subsidiary of Honeywell International Inc., for the U.S. Department of Energy's National Nuclear Security Administration under contract DE-NA0003525.

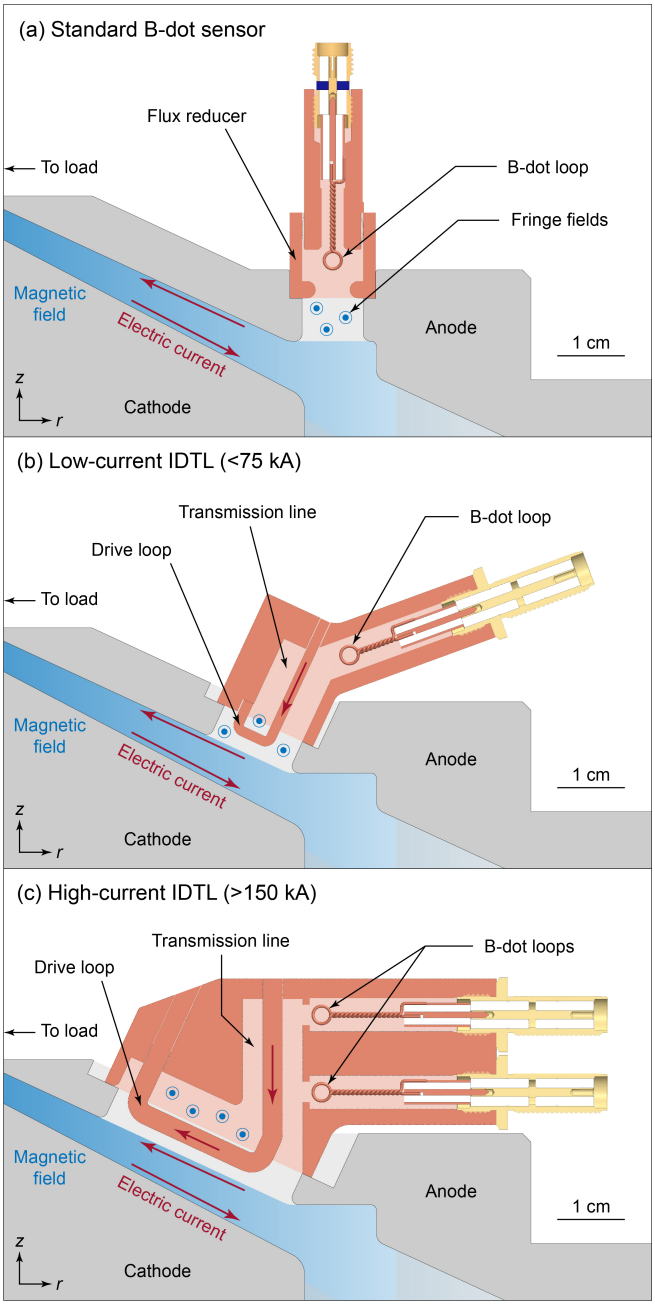

FIG. 1. (a) Schematic of a conical final feed on Z showing the anode, the cathode, and a standard Z B-dot sensor.[13] The B-dot sensor, which is mounted to an azimuthally localized hole in the anode, measures the final feed current by sampling the fringe magnetic fields that form in the anode hole. (b) Schematic of a low-current IDTL that mounts to an enlarged anode hole. Its copper drive loop extends downward into the hole and robustly couples to the available fringe magnetic fields. This coupling drives ~65 kA of secondary current into the short coaxial transmission line embedded in the IDTL body. Two B-dot loops (only one of which is shown since the other is out-of-plane) measure the magnetic field in the IDTL. (c) Schematic of a high-current IDTL that mounts to an elongated anode slot. The slot accommodates a larger drive loop that couples substantially more magnetic flux to the IDTL and generates ~170 kA of secondary current.

Parameter	Formula	IDTL 1b	IDTL 1c
Coupled flux	Φ_Z	0.47 mWb	2.2 mWb
Self inductance	L	7.2 nH	13 nH
Induced current	$I \simeq \Phi_Z/L$	65 kA	170 kA
Magnetic energy	$W_m = \frac{1}{2}LI^2$	15 J	190 J
Induced voltage	$V \simeq 2\omega\Phi_Z$	15 kV	69 kV
Impedance	$Z \simeq V/I$	0.23 Ω	0.41 Ω
Resistance	R	7.2 mΩ	13 mΩ
Skin time	$\tau = L/R$	1.0 µs	1.0 µs
Phase parameter	$2\omega\tau$	31	32
Phase delay	$t_{delay} \simeq (4\omega^2\tau)^{-1}$	1.0 ns	1.0 ns

TABLE I. IDTL circuit parameters when driven with a 20 MA, 100 ns sine-squared current pulse. The angular frequency $\omega = 2\pi f$ is defined using $f = 2.5$ MHz for a 100 ns rise time. Parameters such as the coupled flux Φ_Z, the self-inductance L, and the resistance R are obtained from ANSYS MAXWELL 3D modeling.

where Φ_Z is the magnetic flux from Z coupled to the IDTL drive loop, M_Z is the mutual inductance between Z and the IDTL, I_Z is the Z current, R is the IDTL resistance, and L is the IDTL self-inductance. If we approximate the shape of the Z current pulse as $I_Z \sim \sin^2(\omega t)$ where $\omega = 2\pi f$ and $f = 2.5$ MHz for a 100 ns rise time,[14] then the excitation of the IDTL can be approximated as $d/dt \sim 2\omega i$ and Eq.1 can be solved for the IDTL current:

$$I \simeq \left[\frac{2\omega\tau}{i - 2\omega\tau}\right]\frac{\Phi_Z}{L}, \tag{2}$$

where we have defined $\tau \equiv L/R$ as the skin time of the IDTL. As we will show, IDTLs operate near the perfectly conducting limit where $2\omega\tau \gg 1$ such that the current induced in the IDTL is nearly in-phase with the Z current and is given by $I \simeq -\Phi_Z/L$.

Since the IDTL is fundamentally a three-dimensional object, electromagnetic modeling is required to determine the values of the various circuit parameters in Eq. 1 and 2. We therefore use ANSYS MAXWELL 3D[15] to conduct a 2ω harmonic analysis to determine the expected electromagnetic performance of the two IDTLs in Fig. 1. The resulting modeled circuit parameters are listed in Table I. As expected, the high-current IDTL couples nearly fives times more flux than the low-current IDTL. However, it generates less than three times the current because the larger drive loop increases the self-inductance by nearly a factor of two. Table I also shows that both IDTLs do in fact operate near the perfectly conducting limit such that $2\omega\tau \gg 1$ and the IDTL current is nearly in phase with the Z current ($t_{delay} \simeq 1$ ns). We now proceed to demonstrate that IDTLs are able to achieve their modeled performance when fielded on Z.

III. INITIAL EXPERIMENTAL RESULTS

In this section, we present B-dot sensor results from three Z experiments that fielded low-current IDTLs and

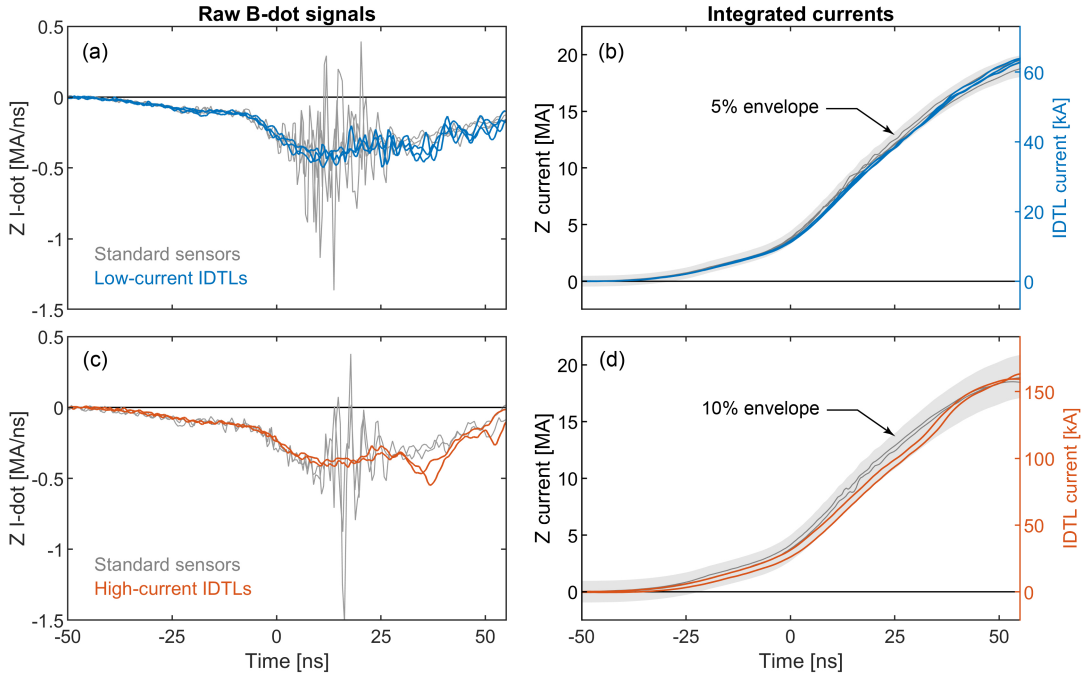

FIG. 2. Demonstration of IDTL performance across five similar Z experiments. The top row shows (a) raw B-dot signals and (b) integrated currents from three experiments that fielded low-current IDTLs, while the bottom row shows (c) raw B-dot signals and (d) integrated currents from two experiments that fielded high-current IDTLs. First, the raw signals from the IDTL B-dot loops are notably cleaner in all cases than the corresponding raw signals from the standard Z B-dot sensors. This indicates that the IDTL B-dot loops may be better protected than the standard loops from the harsh power flow environment in the final feed (see Section IV). Second, the integrated IDTL currents, which are obtained by applying the calibration procedure in Eq. 3, track the standard-sensor currents to within 5% in the low-current IDTL case and 10% in the high-current IDTL case. As such, we conclude that, in spite of the harsh power flow environment on Z, nearly all of the expected current is coupled to both the low- and high-current IDTLs (see the 'IDTL current' axes on the far right).

two that fielded high-current IDTLs. Figures 2a and 2c compare the raw signals from the IDTL B-dot loops (in blue and red, respectively) to those from the standard B-dot sensors (in gray). In both the low- and high-current cases, the IDTL B-dot loops generate cleaner voltage waveforms than do the standard sensors. This observation, which indicates that IDTLs could be used to make high-fidelity measurements of the final feed current, is addressed in Section IV. To understand how to relate the raw B-dot senor signals to the current in the final feed, both the standard sensors and the IDTLs are subjected to a benchtop calibration procedure prior to being fielded on Z.[13] In this procedure, the final feed is driven with an ∼8 kA, 150 ns current pulse that induces millivolt-scale signals on the B-dot loops. Since the calibration current pulse is measured independently by a current-viewing resistor, the induced voltages can be related to the final feed current I_Z using the two-parameter integration procedure described in Wagoner *et al.*[13]:

$$I_Z(t) = \frac{1}{M_Z}\int_{-\infty}^{t} dt'\, V_B(t')\, e^{-(t-t')/\tau_f}, \qquad (3)$$

where V_B is the measured B-dot voltage waveform and the two scalar calibration parameters are M_Z, which is the mutual inductance between the B-dot loop and Z, and τ_f, which is the so-called flux penetration time that accounts for the decay of currents that are induced in conductors near the B-dot loop. Typical values for these calibration parameters are $M_Z \sim 0.1$ pH and $\tau_f \sim 0.7$–1.1 µs. In practice, a nonlinear fit to the calibration data is conducted for each B-dot loop. The resulting M_Z and τ_f values are then applied to the voltage waveforms that are acquired on the actual Z experiment.

Figures 2b and 2d compare the integrated currents inferred from the IDTLs to those from the standard B-dot sensors. In the low-current case (Fig. 2b), the IDTL-inferred currents track the standard-sensor currents to within 5%, which is the quoted accuracy of the standard sensors.[13] This indicates that the low-current IDTLs are losslessly coupling the full amount of expected current as shown on the blue 'IDTL current' axis on the far right. In the high-current case (Fig. 2d), the IDTL-inferred currents track the standard-sensor current to within 10%. A small amount of IDTL current loss is observed during the rise on both of the high-current IDTL shots, but the loss appears to clear as Z approaches peak current such that the high-current IDTLs also couple the full amount of expected current (see the red 'IDTL current' axis on the far right). Importantly, the primary loads on all five of the Z experiments shown in Fig. 2 performed nominally according to both driver-target coupling diagnostics and

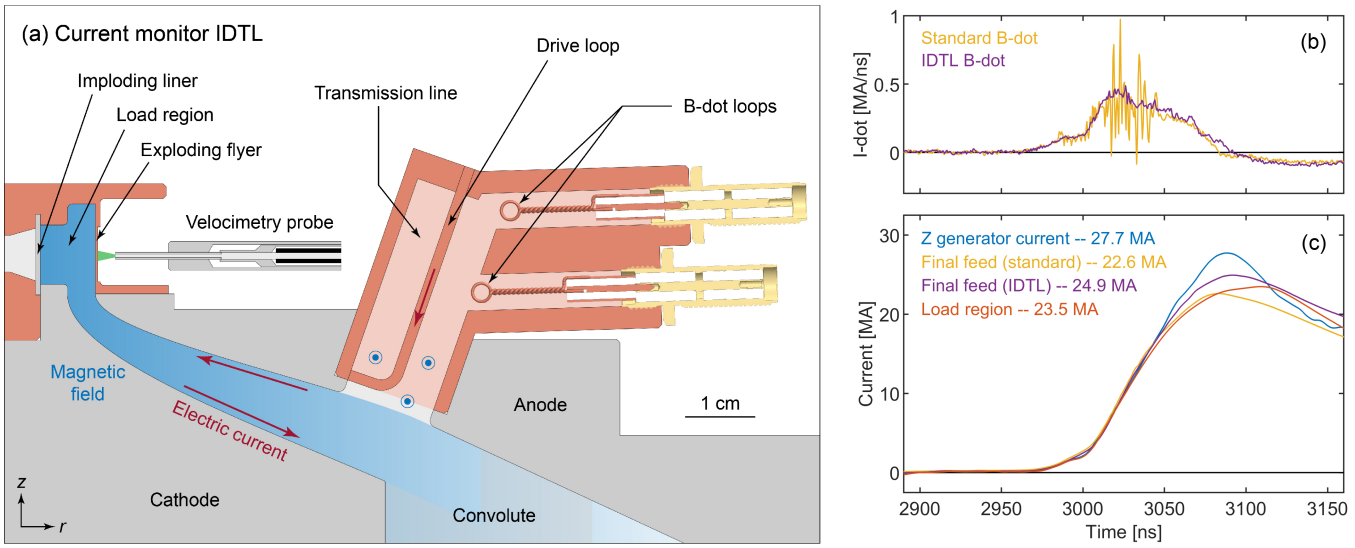

FIG. 3. (a) Schematic depicting a streamlined design for a current monitor IDTL that has been fielded dozens of times on Z. Rather than looping down and back up within the anode hole, the drive loop now terminates horizontally into the side wall of the 13 mm bore of the IDTL. This simplifies construction and increases standoff to promote lossless current coupling. To the left of the IDTL, a fiber-coupled velocimetry probe measures the magnetically driven explosion of a copper flyer to determine the current delivered to load region.[16] (b) Raw signals from a standard B-dot sensor (yellow) and an IDTL B-dot loop (purple). (c) Integrated final feed currents from the standard sensor (yellow) and the IDTL (purple). Only the IDTL waveform remains causal with respect to the generator current (blue) and velocimetry-based load current (red). See the text for further details.

other metrics. This key result demonstrates that IDTLs can non-perturbatively generate >150 kA of secondary current at 20 MA on Z, which is enough to drive an X-pinch in parallel with the primary load.[11]

While the results presented in Fig. 2 demonstrate that IDTL current coupling is nearly lossless on Z, they do not provide direct measurements of the current flowing in the IDTLs (modeled values are used instead). This is because the benchtop calibration procedure in Eq. 3 does not distinguish the magnetic fields that are generated by the IDTL from those generated by Z itself. Comparing the amplitudes of the measured IDTL B-dot voltages to expectations from Ansys Maxwell 3D yields agreement to within ∼50%, but such comparisons are highly sensitive to the as-built dimensions and positions of the IDTL B-dot loops. In the future, we expect that better metrology of the as-built IDTL B-dot loops would provide more precise measurements of the IDTL current.

IV. CURRENT MONITOR IDTLS

While the focus to this point has been on whether IDTLs can non-perturbatively generate enough secondary current to drive an X-pinch, the raw IDTL B-dot loop signals shown in Fig. 2a reveal a second important diagnostic application for IDTLs: as improved final feed current monitors. When compared to the raw signals from the standard B-dot sensors, the IDTL signals in Fig. 2a are noticeably void of strong voltage oscillations that are routinely observed on standard B-dot sensors in the final feed. We hypothesize that IDTLs produce cleaner signals for two reasons: (1) the IDTL drive loop acts as a low-pass filter and is therefore less sensitive to high-frequency magnetic fluctuations in the anode cavity; and (2) IDTLs better protect their B-dot loops from particle and radiation bombardment by eliminating the direct line-of-sight between the B-dot loops and the final feed. Thus, if an IDTL can achieve sufficiently lossless current coupling, it would generate cleaner, higher-fidelity final feed current measurements.

Figure 3a shows the schematic of a streamlined current monitor IDTL design that has been fielded dozens of times on Z. The drive loop now terminates directly into the side wall of the 13 mm bore of the IDTL, which both simplifies construction and improves standoff to promote lossless current coupling. Figure 3b compares the raw signal generated by one of these IDTLs to the raw signal from a standard B-dot sensor on the same Z experiment. As before, the IDTL signal is noticeably void of spurious voltage oscillations. To compare the final feed currents inferred from these two types of sensors, we integrate the B-dot voltages using Eq. 3 and plot the results in Fig. 3c. The IDTL current waveform (purple) exceeds the standard-sensor waveform (yellow) by 2.3 MA or 10%, which indicates that the differences between the raw signals in Fig. 3b meaningfully impact the inferred current.

To assess the accuracy of the standard-sensor and IDTL-based current measurements shown in Fig. 3c, we examine two other current measurements from the same Z experiment. First, the 'Z generator current' represents the current delivered to the entrance of the double post-hole convolute,[17,18] which is a three-dimensional struc-

ture at $r \sim 7.5\,\mathrm{cm}$ that combines four parallel outer transmission lines into the single final power feed discussed throughout this paper. The Z generator current is constructed by losslessly translating current and voltage measurements made at the vacuum insulator stack[13] to the entrance of the double post-hole convolute.[19] While current can be lost in the convolute,[20] it cannot be created. As such, the true final feed current must run below the generator current to remain causal. The second current waveform of interest is the 'load region' current that is measured using velocimetry techniques.[16] Since the load region is downstream from the final feed, the final feed current must run above the load current to remain causal. In summary, the final feed current must be bracketed from above by the Z generator current and from below by the load region current.

Most interestingly, the IDTL-based final feed current waveform shown in Fig. 3c satisfies these causality conditions while the standard-sensor waveform does not. Although a multi-MA disparity between IDTL-inferred currents and standard-sensor currents is not always observed (see Fig. 2 for example), the causality issues identified here do routinely appear, especially on higher inductance experiments that generate harsher conditions in the final feed. Due to their apparent resiliency to these harsh conditions, current monitor IDTLs are being pursued as a potential replacement for the standard Z B-dot sensors.

V. SUMMARY

The inductively driven transmission line (IDTL) is a passively coupled device that redirects a small amount of the magnetic energy in the final feed of Z along a secondary path to ground. Initial IDTL experiments and modeling indicate that IDTLs operate non-perturbatively and that they can draw $>150\,\mathrm{kA}$ of secondary current, which makes them the first device capable of driving an X-pinch in parallel with the primary load on Z. Experiments are presently underway to develop IDTL-powered X-pinches, and initial results indicate that IDTLs can successfully drive an X-pinch in spite of the increased impedance of the X-pinch load. Experimental results presented in this paper also indicate that IDTLs can generate cleaner, higher-fidelity measurements of the final feed current. Efforts are underway to test and improve the reliability and resiliency of current monitor IDTLs so that they can be implemented as a new workhorse current monitor on Z.

ACKNOWLEDGMENTS

The authors thank Mark Savage and Ronald Mourning for their assistance with B-dot sensor calibrations and Katherine Chandler, Brian Hutsel, and David Ampleford for useful discussions. We also thank the load hardware engineers and operations staff at Z for their contributions to fielding IDTLs on numerous experiments. This work was supported by the Laboratory Directed Research and Development program at Sandia National Laboratories, a multimission laboratory managed and operated by National Technology and Engineering Solutions of Sandia LLC, a wholly owned subsidiary of Honeywell International Inc. for the U.S. Department of Energy's National Nuclear Security Administration under contract DE-NA0003525. This article describes objective technical results and analysis. Any subjective views or opinions that might be expressed in the article do not necessarily represent the views of the U.S. Department of Energy or the U.S. Government. The data that support the findings of this study are available from the corresponding author upon reasonable request.

[1] D. B. Sinars, M. A. Sweeney, C. S. Alexander, D. J. Ampleford, T. Ao, J. P. Apruzese, C. Aragon, D. J. Armstrong, K. N. Austin, T. J. Awe, *et al.*, Phys. Plasmas **27**, 070501 (2020).
[2] S. M. Zakharov, G. V. Ivanenkov, A. A. Kolomenskii, S. A. Pikuz, A. I. Samokhin, and J. Ullschmeid, Sov. Tech. Phys. Lett. **8**, 456 (1982).
[3] S. A. Pikuz, T. A. Shelkovenko, and D. A. Hammer, Plasma Phys. Reports **41**, 445 (2015).
[4] D. H. Kalantar and D. A. Hammer, Phys. Rev. Lett. **71**, 3806 (1993).
[5] S. A. Pikuz, T. A. Shelkovenko, V. M. Romanova, D. A. Hammer, A. Y. Faenov, V. A. Dyakin, and T. A. Pikuz, Rev. Sci. Instr. **68**, 740 (1997).
[6] S. V. Lebedev, F. N. Beg, S. N. Bland, J. P. Chittenden, A. E. Dangor, M. G. Haines, M. Zakaullah, S. A. Pikuz, T. A. Shelkovenko, and D. A. Hammer, Rev. Sci. Instr. **72**, 671 (2001).
[7] T. A. Shelkovenko, S. A. Pikuz, and D. A. Hammer, Plasma Phys. Reports **42**, 226 (2016).
[8] F. Zucchini, S. N. Bland, C. Chauvin, P. Combes, D. Sol, A. Loyen, B. Roques, and J. Grunenwald, Rev. Sci. Instr. **86**, 033507 (2015).
[9] S. V. Lebedev, F. N. Beg, S. N. Bland, J. P. Chittenden, A. E. Dangor, M. G. Haines, S. A. Pikuz, and T. A. Shelkovenko, Phys. Rev. Lett. **85**, 98 (2000).
[10] F. N. Beg, K. Krushelnick, P. Lichtsteiner, A. Meakins, A. Kennedy, N. Kajumba, G. Burt, and A. E. Dangor, Appl. Phys. Lett. **82**, 4602 (2003).
[11] T. A. Shelkovenko, S. A. Pikuz, J. D. Douglass, R. D. Mcbride, J. B. Greenly, and D. A. Hammer, IEEE Trans. Plasma Sci. **34**, 2336 (2006).
[12] J. D. Douglass and D. A. Hammer, Rev. Sci. Instr. **79**, 033503 (2008).
[13] T. C. Wagoner, W. A. Stygar, H. C. Ives, T. L. Gilliland, R. B. Spielman, M. F. Johnson, P. G. Reynolds, J. K. Moore, R. L. Mourning, D. L. Fehl, *et al.*, Phys. Rev. ST Accel. Beams **11**, 100401 (2008).
[14] M. E. Savage, K. R. LeChien, M. R. Lopez, B. S. Stoltzfus, W. A. Stygar, D. S. Artery, J. A. Lott, and P. A. Corcoran, in *2011 IEEE Pulsed Power Conference* (2011) pp. 983–990.
[15] Ansys® Electronics Desktop 2018.2.
[16] A. Porwitzky and J. Brown, Phys. Plasmas **25**, 063102 (2018).
[17] R. B. Spielman, P. Corcoran, J. Fockler, H. Kishi, and P. W. Spence, in *7th Pulsed Power Conference* (1989) pp. 445–448.
[18] T. D. Pointon, W. A. Stygar, R. B. Spielman, H. C. Ives, and K. W. Struve, Phys. Plasmas **8**, 4534 (2001).
[19] C. A. Jennings, J. P. Chittenden, M. E. Cuneo, W. A. Stygar, D. J. Ampleford, E. M. Waisman, M. Jones, M. E. Savage, K. R. LeChien, and T. C. Wagoner, IEEE Trans. Plasma Sci. **38**, 529 (2010).
[20] B. T. Hutsel, P. A. Corcoran, M. E. Cuneo, M. R. Gomez, M. H. Hess, D. D. Hinshelwood, C. A. Jennings, G. R. Laity, D. C. Lamppa, R. D. McBride, *et al.*, Phys. Rev. Accel. Beams **21**, 030401 (2018).